THE EUROPEAN
PHYSICAL JOURNAL A

Regular Article – Experimental Physics

Studies of continuum states in ^{16}Ne using three-body correlation techniques

J. Marganiec[1,2,3], F. Wamers[1,2,3,4], F. Aksouh[2,a], Yu. Aksyutina[2], H. Álvarez-Pol[5], T. Aumann[1,2], S. Beceiro-Novo[5], K. Boretzky[2], M.J.G. Borge[6,7], M. Chartier[8], A. Chatillon[2], L.V. Chulkov[2,9], D. Cortina-Gil[5], H. Emling[2], O. Ershova[2,10], L.M. Fraile[11], H.O.U. Fynbo[12], D. Galaviz[7], H. Geissel[2], M. Heil[2], D.H.H. Hoffmann[1], J. Hoffmann[2], H.T. Johansson[13], B. Jonson[13], C. Karagiannis[2], O.A. Kiselev[2], J.V. Kratz[14], R. Kulessa[15], N. Kurz[2], C. Langer[2,10], M. Lantz[16], T. Le Bleis[2,17], R. Lemmon[18], Yu.A. Litvinov[2], K. Mahata[2,19], C. Müntz[2], T. Nilsson[13], C. Nociforo[2], G. Nyman[13], W. Ott[2], V. Panin[1,2], S. Paschalis[1,8], A. Perea[7], R. Plag[2,10], R. Reifarth[2,10], A. Richter[1], C. Rodriguez-Tajes[5], D. Rossi[2,b], K. Riisager[12], D. Savran[3,4], G. Schrieder[1], H. Simon[2], J. Stroth[10], K. Sümmerer[2], O. Tengblad[7], H. Weick[2], M. Wiescher[20], C. Wimmer[2,10], and M.V. Zhukov[13]

1   Institut für Kernphysik, Technische Universität Darmstadt, D-64289 Darmstadt, Germany
2   GSI Helmholtzzentrum für Schwerionenforschung GmbH, D-64291 Darmstadt, Germany
3   ExtreMe Matter Institute EMMI and Research Division GSI, D-64291 Darmstadt, Germany
4   Frankfurt Institute for Advanced Studies FIAS, D-60438 Frankfurt am Main, Germany
5   Grupo de Física Nuclear, Universidade de Santiago de Compostela, ES-15782 Santiago de Compostela, Spain
6   ISOLDE-EP, CERN, CH-1211 - Geneva-23, Switzerland
7   Instituto de Estructura de la Materia, CSIC, ES-28006 Madrid, Spain
8   Department of Physics, University of Liverpool, Liverpool L69 3BX, UK
9   Kurchatov Institute, RU-123182 Moscow, Russia
10 Institut für Angewandte Physik, Goethe Universität, D-60438 Frankfurt am Main, Germany
11 Grupo de Física Nuclear, FAMN, Universidad Complutense de Madrid, CEI Moncloa, ES-28040 Madrid, Spain
12 Department of Physics and Astronomy, University of Aarhus, DK-8000 Aarhus, Denmark
13 Fundamental Fysik, Chalmers Tekniska Högskola, SE-412 96 Göteborg, Sweden
14 Institut für Kernchemie, Johannes Gutenberg-Universität Mainz, D-55122 Mainz, Germany
15 Instytut Fizyki, Uniwersytet Jagelloński, PL-30-059 Kraków, Poland
16 Institutionen för fysik och astronomi, Uppsala Universitet, SE-75120 Uppsala, Sweden
17 Physik-Department E12, Technische Universität München, D-85748 Garching, Germany
18 Nuclear Physics Group, STFC Daresbury Lab, Warrington WA44AD, Cheshire, UK
19 Nuclear Physics Division, Bhabha Atomic Research Centre, Trombay, Mumbai-400 085, India
20 JINA, University of Notre Dame, Notre Dame, IN 46556, USA

Abstract. Two-proton decay of the unbound $T_z = -2$ nucleus ^{16}Ne, produced in one-neutron knock-out from a 500 MeV/u ^{17}Ne beam, has been studied at GSI. The ground state, at a resonance energy 1.388(15) MeV, ($\Gamma = 0.082(15)$ MeV) above the ^{14}O+p+p threshold, and two narrow resonances at $E_r = 3.220(46)$ MeV and 7.57(6) MeV have been investigated. A comparison of the energy difference between the first excited 2^+ state and the 0^+ ground state in ^{16}Ne with its mirror nucleus ^{16}C reveals a small Thomas-Ehrman shift (TES) of +70(46) keV. A trend of the TES for the $T = 2$ quintet is obtained by completing the known data with a prediction for ^{16}F obtained from an IMME analysis. The decay mechanisms of the observed three resonances were revealed from an analysis of the energy and angular correlations of the ^{14}O+p+p decay products. The ground state decay can be considered as a genuine three-body (democratic) mode and the excited states decay sequentially via states in the intermediate nucleus ^{15}F, the 3.22 MeV state predominantly via the ^{15}F ground-state resonance, while the 7.57 MeV state decays via the $5/2^+$ resonance in ^{15}F at 2.8 MeV above the ^{14}O+p+p threshold. Further, from an analysis of angular correlations, the spin-parity of the 7.57 MeV state has been determined as $I^\pi = 2^+$ and assigned as the third 2^+ state in ^{16}Ne based on a comparison with ^{16}C.

a   *Present address*: Dept of Physics and Astronomy, College of Science, King Saud University, 11451 Riyadh, KSA.
b   *Present address*: National Superconducting Cyclotron Laboratory, MSU, East Lansing, MI 48824, USA.

1 Introduction

This paper presents a detailed analysis of experimental data for the unbound nucleus ^{16}Ne obtained in one-neutron knockout reactions from a relativistic ^{17}Ne beam at GSI. In this experiment the first observation of the unbound $T_z = -5/2$ nucleus ^{15}Ne, produced in two-neutron knockout reactions, could also be done and this result was published recently [1]. Some results for ^{16}Ne were given in Ref. [1] and here we emphasise in particular what one may learn about ^{16}Ne from a study of energy and angular correlations in its two-proton decay to ^{14}O.
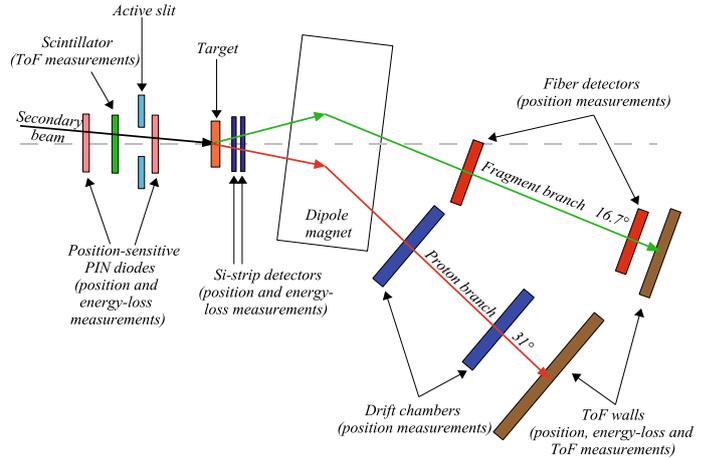
2 Earlier studies of ^{16}Ne

The unbound isotope ^{16}Ne was first observed in an experiment performed at LAMPF in 1977 by Holt *et al.* [2]. This experiment was followed by a series of studies of ^{16}Ne using pion double-charge exchange reactions [2–4] or four-neutron pick-up reactions [5,6]. The first excited state was found at an excitation energy $E^* = 1.69(7)$ MeV [5] and assigned as a 2^+ state, based on mirror symmetry. Föhl *et al.* [4] observed an excited state at $E^* = 2.1(2)$ MeV and interpreted it as the second 0^+ state. In a more recent experiment with ^{16}Ne, produced in one-neutron knockout reactions from ^{17}Ne, a narrow excited state at $E^* = 6.25$ MeV [7,8] was observed. In the course of writing this paper a new experiment performed at MSU appeared as a web publication [9]. A summary of the experimental data in the literature is given in table 1 together with the results from this experiment.
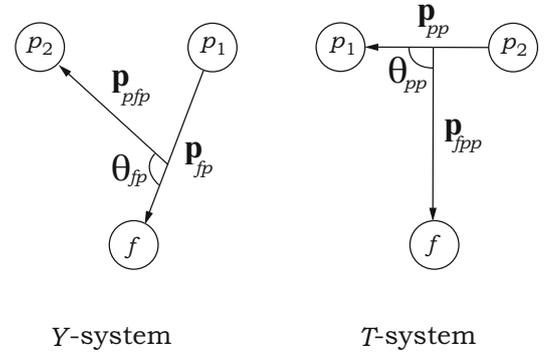
3 Experiment

As mentioned above the present data were obtained in an experiment performed at GSI [1] where the unbound ^{16}Ne nuclei were produced in one-neutron knockout reactions from a secondary ^{17}Ne beam. The beam, with an energy of around 500 MeV/u, was directed towards carbon, 370 mg/cm^2, or polyethylene, 213 mg/cm^2, reaction targets. The reaction products were identified by measuring their energy losses and positions, using two Si-strip detectors placed directly behind the reaction target. The reaction products were subsequently separated according to mass and charge by the magnetic field of a large-gap dipole magnet (ALADIN). The protons (p) and heavy fragments (f) were guided into two branches. The heavy ions were measured using two scintillating-fibre arrays and a two-layer Time-of-Flight (ToF) wall, while the protons were detected using two multi-wire drift chambers and a ToF wall. With these different detector combinations, position, energy loss, and ToF data were obtained. A schematic outline of the setup is given in fig. 1.

Coincidences between ^{14}O and two protons, having velocities close to the beam velocity, provided the momentum four vectors used in the analysis. The momentum vectors were transformed into the projectile rest-mass frame

Fig. 1. Schematic outline of the experimental setup. For details see text.

Fig. 2. Jacobi coordinates for the three-body $f + p + p$ system.

where two different sets of non-relativistic Jacobi coordinates were used as shown in fig. 2.

i) A system referred to as the Y-system, where θ_{fp} is the angle between the two vectors $\mathbf{p}_{fp}$ and $\mathbf{p}_{p-fp}$;

$$\mathbf{p}_{fp} = \left(\frac{\mathbf{p}_f}{m_f} - \frac{\mathbf{p}_1}{m_p} \right) \frac{m_f m_p}{m_f + m_p},$$
$$\mathbf{p}_{p-fp} = \left(\frac{\mathbf{p}_2}{m_p} - \frac{\mathbf{p}_f + \mathbf{p}_1}{m_f + m_p} \right) \frac{m_p(m_f + m_p)}{m_f + 2m_p}; \quad (1)$$

ii) and a T-system, where θ_{pp} is the angle between $\mathbf{p}_{pp}$ and $\mathbf{p}_{f-pp}$,

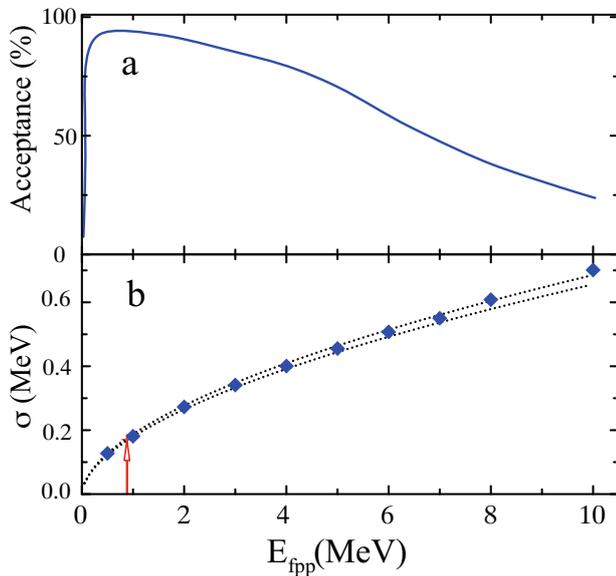$$\mathbf{p}_{pp} = \frac{1}{2} \left(\mathbf{p}_1 - \mathbf{p}_2 \right),$$
$$\mathbf{p}_{f-pp} = \left(\frac{\mathbf{p}_f}{m_f} - \frac{\mathbf{p}_1 + \mathbf{p}_2}{2m_p} \right) \frac{2m_f m_p}{m_f + 2m_p}. \quad (2)$$

The internal kinetic energy, that is, the relative energy, E_{fpp}, in the three-body ^{14}O+p+p system, as well as the fractional energies in the fragment-proton ($\epsilon_{fp} = E_{fp}/E_{fpp}$) and the proton-proton ($\epsilon_{pp} = E_{pp}/E_{fpp}$) sub-systems, were determined. The correlation functions normalised to unity, for the fractional-energy distributions

Table 1. Resonance energies (E_r) and widths (Γ) in MeV of ^{16}Ne states above the ^{14}O+p+p threshold.

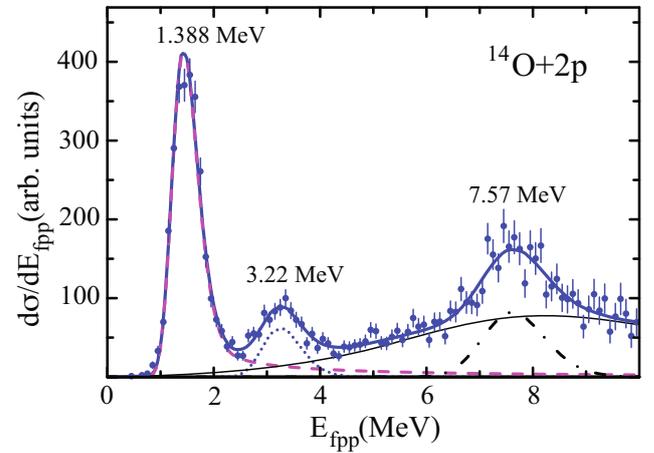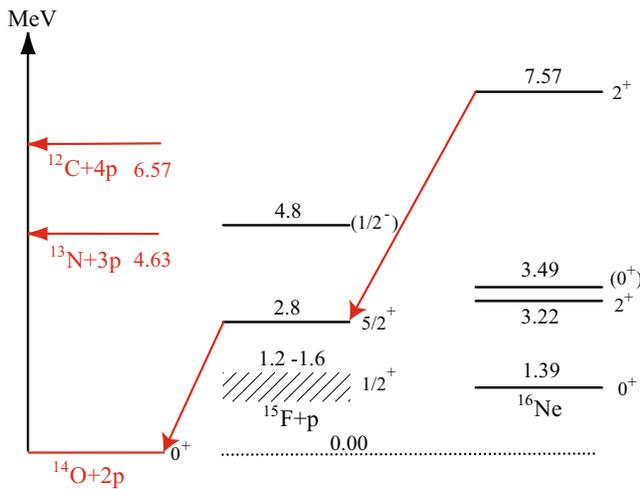| Reaction | Beam energy | Ground state, $I^\pi = 0^+$ | | $I^\pi = (0^+, 2^+)$ | | $I^\pi = (2^+)$ | | Ref. |
		E_r	Γ	E_r	Γ	E_r	Γ	
^{16}O(π^+, π^-)	145 MeV	1.8(5)	–	–	–	–	–	[2]
^{16}O(π^+, π^-)	180 MeV	1.466(45)	–	–	–	–	–	[3]
^{16}O(π^+, π^-)	45–90 MeV	–	–	3.5(2)	–	–	–	[4]
^{20}Ne$(^4$He,^{8}He)	117 MeV	1.33(8)	0.2(1)	3.02(11)	–	–	–	[5]
^{20}Ne$(^4$He,^{8}He)	129 MeV	1.399(24)	0.11(4)	–	–	–	–	[6]
Be$(^{17}$Ne,2p^{14}O)	450 MeV/u	1.35(8)	–	3.2(2)	0.2(2)	7.6(2)	0.8$(^{+4}_{-8})$	[7,8]
Be$(^{17}$Ne,2p^{14}O)	57.6 MeV/u	1.466(20)	< 0.080	–	–	–	–	[9]
C,CH$_2$(^{17}Ne,2p^{14}O)	500 MeV/u	1.388(15)	0.082(15)	3.220(46)	$\leq$ 0.05	7.57(6)	$\leq$ 0.1	(a)

(a) This experiment.

Fig. 3. (a) The overall acceptance. (b) The experimental resolution σ as a function of the internal kinetic energy E_{fpp}. The results of the Monte Carlo simulations are shown as diamonds. The dotted lines show the deviations by $\pm 2.2\%$ from $\sigma = 0.183 \cdot E_{fpp}^{0.563}$. The arrow indicates the energy of the benchmark point (see text for explanations).

$W(\epsilon_{fp})$ and $W(\epsilon_{pp})$ as well as the angular distributions $W(\cos\theta_{fp})$ and $W(\cos\theta_{pp})$, were constructed and analysed. The analysis was done by making two loops through the collected events, by choosing one detected proton as the first proton in the first loop and changing to the other in the second loop.

Figure 3(a) shows the overall acceptance, including the resolving power of the proton-tracking routine and the geometrical acceptance of the setup, obtained in Monte Carlo simulations as described in ref. [1]. The ^{14}O+p+p relative energy spectrum, shown in fig. 4 was corrected for this acceptance. The Monte Carlo simulations were also used to get the response function of the experimental setup by reproducing a case with zero-width resonances in the

Fig. 4. ^{14}O+p+p relative energy spectrum. The spectrum is decomposed into three Breit-Wigner shaped resonances (dashed, dotted and dash-dotted curves). The thin black line extending below the spectrum is interpreted as a contribution from several unresolved resonances. The full drawn blue curve is the sum of all components. (From fig. 3 of ref. [1]).

^{14,15}O+2p systems at resonance energies between 0.5 to 10 MeV. The reconstructed resonances were well described as Gaussians: $A \cdot \exp(-(E_{fpp} - \Delta - E_i)^2 / 2\sigma_i^2)$, where E_i is the input probe energy. The experimental resolution σ_i and the energy offset Δ are parameters of the fit. The 2p decay of the narrow $5/2^-$ state in ^{17}Ne [10] was used as a benchmark for adjusting both σ and Δ (see ref. [1]). The obtained σ_i values are shown in fig. 3(b) as diamonds. Finally, the set of σ_i values was fitted by an exponential function. This resulted in a response-function with $\Delta = 50(13)$ keV and $\sigma = 0.183(4) \cdot E_{fpp}^{0.563}$. The statistical accuracy of the obtained dispersion parameter $\delta\sigma/\sigma = 2.2\%$ allows an effective folding of a theoretical spectrum with the response function in the fitting procedures. This least-squares fitting was performed using the function minimisation and error analysis code MINUIT [11].
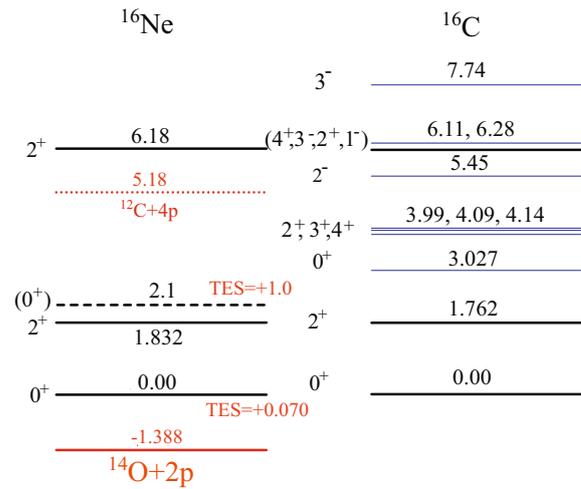
Fig. 5. Energies of ground states and excited states in ^{16}Ne and ^{15}F+p relative to ^{14}O+2p threshold.

4 Analysis

The experimental ^{14}O+p+p relative-energy spectrum, shown in fig. 4, was analysed by assuming that the resonances could be described with Breit-Wigner shapes, in which the width was energy-dependent and by using the analytic form of the response as described in sect. 3. The energy dependence of the width is important only for the ground state, while the shapes of the other resonances are dominantly determined by the experimental resolution. A simplified version of the model for sequential proton emission, explained in details below in eqs. (4), was used. The simplification was based on experimental observation that $W(\epsilon_{fp})$ is a narrow distribution centred at $E_{fp} = E_{fpp}/2$ (see fig. 7(a)). Then, as the first approximation the function $\rho(E_{fp})$ in eqs. (4) can be taken equal to $\delta(E_{fp} - E_{fpp}/2)$, where δ is the Dirac delta function. This simplification reduces essentially the computing time.

The analysis reveals three sharp resonances together with a broad distribution ranging from low energy up to the end of the spectrum. This latter distribution is interpreted as a contribution from several unresolved resonances. The energies and widths of the three resonances observed in this experiment are given in table 1. For the ground state a width of 82 keV with a statistical accuracy of 10 keV was obtained. By varying the factor in the expression for σ by 2.2% an additional systematic error of 5 keV is obtained and gives the final result of $\Gamma = 82(15)$ keV. Figure 5 shows the positions of the ^{16}Ne states and the ^{15}F+p states relative to the ^{14}O+p+p threshold.

The most surprising result obtained for ^{16}Ne is the existence of a narrow resonance with very large decay energy, $E_r = 7.57$ MeV, observed for the first time by Mukha *et al.* [7,8]. They gave a tentative assignment of $I^\pi = 2^+$ to this state. Below, it will be shown that the spin and parity can be determined unambiguously from an analysis of the three-body correlations between the ^{14}O+p+p decay products.

Fig. 6. Comparison of the level positions in the mirror nuclei ^{16}Ne and ^{16}C. The first excited state in ^{16}Ne and the corresponding state in ^{16}C are drawn at the same energy. The thin lines denote states observed experimentally in ^{16}C but not seen in ^{16}Ne. The energies of the ^{16}C levels were taken from refs. [13–15]. The red dotted line is the ^{12}C+4p threshold. TES stands for Thomas-Ehrman shift.

4.1 Mirror states and Thomas-Ehrman shift

A comparison between the ^{16}Ne level scheme, based on the results presented here, and that of its well-known mirror nucleus, ^{16}C, is shown in fig. 6. The large number of states observed in ^{16}C might indicate the presence of three times more resonance states in ^{16}Ne than those observed in the present experiment.

The position of the ^{16}Ne ground-state resonance and its width are both in a good agreement with earlier results, but with superior precision due to better statistics and energy calibration. However, the obtained width, $\Gamma = 82(15)$ keV, is essentially larger than calculated in a three-body model, which predicts $\Gamma = 0.8^{+2.3}_{-0.65}$ keV [12]. As a simple check, the ^{17}Ne($5/2^-$) state and ^{16}Ne(g.s.) were fitted with Gaussians. The shape of ^{17}Ne($5/2^-$) state was perfectly described, with $\chi^2/N = 0.899$, while a minimal $\chi^2/N = 1.946$ was obtained for the ^{16}Ne(g.s.). This value allows to conclude, with the confidence level of 95%, that it has not a Gaussian shape. Thus the difference in shapes of the observed peaks in ^{17}Ne($5/2^-$) and ^{16}Ne(g.s.) indicates that the width of ^{16}Ne(g.s.) is non-negligible.

The first excited state was observed at $E^* = 1.69(7)$ MeV [5], close to the known excitation energy of the 2^+ state in the mirror nucleus ^{16}C at $E^* = 1.762(2)$ MeV [13], and was assigned to have $I^\pi = 2^+$. The observed width of the state found in the present experiment at $E^* = 1.832(48)$ MeV is also narrow, suggesting an $I^\pi = 2^+$ assignment.

In ref. [4], a first excited state was found at $E^* = 2.1(2)$ MeV (the energy difference is about 2σ) and interpreted as the mirror state of the ^{16}C(0_2^+) state at $E^* = 3.027$ MeV [13] (see fig. 6). Theoretical calculations have predicted that the excitation energies of the 2_1^+ and

0_2^+ states in ^{16}Ne may be close in energy [16]. If the state observed in ref. [4] is a 0^+ state it would be subject to a large Thomas-Ehrman shift (TES) [17,18] as indicated in fig. 6.

As pointed out in ref. [16], there is, however, a confusion in the literature concerning the definition of the TES. Here, we use it as the difference between the excitation energy differences between mirror states with spins I_1 and I_2:

$$\Delta(I_1, I_2) = [E(I_1) - E(I_2)]_{\mathrm{Ne}} - [E(I_1) - E(I_2)]_{\mathrm{C}}. \quad (3)$$

The energies of the 0^+ and 2^+ in ^{16}Ne obtained here and the corresponding mirror states in ^{16}C (fig. 6), shows that the TES is small, $\Delta(2^+, 0^+) = +70(46)$ keV. This may be compared to the 0^+ and 2^+ shift for the mirror pair ^{18}Ne-^{18}O, which has a similar core+2p structure, which is $\Delta(2^+, 0^+) = -94.77(2)$ keV. Such a negative value of the TES is, however, not expected for nuclei with a core+2N structure. One possible reason for this anomaly in the ^{18}Ne-^{18}O pair may be an excitation out of the p-shell core, see ref. [19] and references therein.

In general, the TES has been explained as mainly originating in the Coulomb-energy difference for different particle orbits. This effect is especially pronounced for s-shell nucleons since their wave functions are spatially more extended. For nuclei with a core+nucleon structure, the TES between a state with a negligible s-shell contribution and a state where the s-shell dominates is always positive. The amount of $(s_{1/2})^2$ configuration in the structure of the ground states in ^{16}Ne-^{16}C is about 46% while it decreases to 19% for ^{18}Ne-^{18}O. The difference in the population of the s-shell explains qualitatively the observed values of the shifts. However, the TES is expected to exhibit an anomalous behaviour in nuclei beyond the proton drip-line since for those further mechanisms for the energy shift are required [20–22]. A profound analysis of the TES can therefore shed more light on the structure of such light nuclei.

4.2 Energy and angular correlations

The two-proton decay of the ^{16}Ne states may be discussed in terms of three extreme scenarios:

- a di-proton decay;
- a sequential decay through the ^{15}F ground-state resonance;
- a genuine three-body decay.

Before discussing the correlation functions for the states in ^{16}Ne, we give here the basic formalism used in the present analysis.

The fractional-energy correlations for sequential decays in the Y-system are treated within an R-matrix formalism described in ref. [23] and we employ the same no-

tations as therein:

$$\frac{\mathrm{d}\sigma}{\mathrm{d}E} \propto \frac{\Gamma_{\mathrm{tot}}(E)}{(E_1 - E)^2 + \Gamma_{\mathrm{tot}}(E)^2/4},$$

$$W(\epsilon) = C \int_0^\infty \frac{\Gamma_1(E, U)}{(E_1 - E)^2 + \Gamma_{\mathrm{tot}}(E)^2/4} \mathrm{d}E,$$

$$\Gamma_1(E, U) = 2\gamma_1^2 P_{l_1}(E - U)\rho(U),$$

$$\rho(U) = c \frac{\Gamma_2(U)}{(E_2 - U)^2 + \Gamma_2(U)^2/4},$$

$$\Gamma_2(U) = 2\gamma_2^2 P_{l_2}(U),$$

$$\Gamma_{\mathrm{tot}}(E) = \int_0^E \Gamma_1(E, U)\mathrm{d}U,$$

$$\epsilon = U/E, \quad (4)$$

where c is chosen to make $\int_0^\infty \rho(U)\mathrm{d}U = 1$ and C to make $\int_0^1 W(\epsilon)\mathrm{d}\epsilon = 1$. E_1 and E_2 are the resonance energies in the initial and intermediate systems. The quantities E and U denote the internal energy in the ^{14}O+p+p system and the energy of the second emitted proton, respectively, and γ_1^2 and γ_2^2 are taken to reproduce the observed widths of the resonances. The penetrability factors $P_l(E)$ are determined as: $P_l = kR/(F_l^2 + G_l^2)$, where F_l and G_l are the regular and irregular Coulomb wave functions.
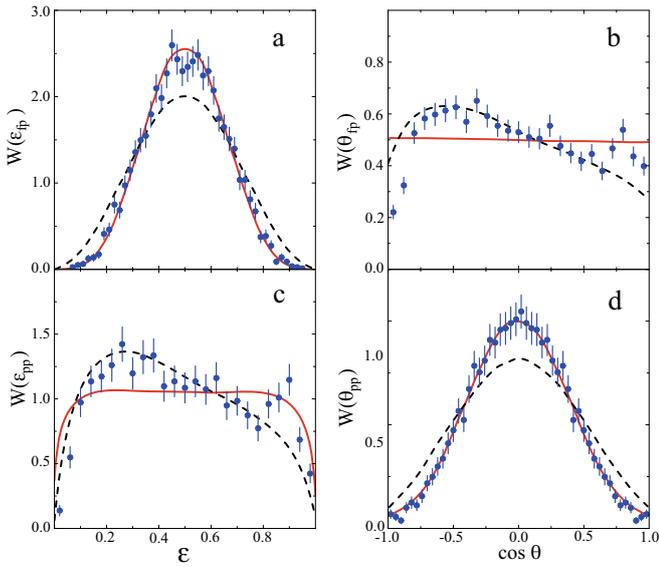
Angular correlation functions $W(\theta)$ were obtained using the formalism proposed in ref. [24] extended for the case with nonzero initial spin I:

$$W(\theta) = \sum_{m_2, \nu_1, \nu_2} N \left[A_{\nu_1, \nu_2} P_{m_2}^{l_2}(\theta) \right]^2,$$

$$A_{\nu_1, \nu_2} = C_{0, \nu_1, \nu_1}^{l_1, s, j_1} C_{m_2, \nu_2, m_2+\nu_2}^{l_2, s, j_2} C_{\nu_1, m_2+\nu_2, M}^{j_1, j_2, I},$$

$$M = m_2 + \nu_1 + \nu_2,$$

$$N = \frac{(2l_1 + 1)(2l_2 + 1)(l_2 - m_2)!}{2(2I + 1)(l_2 + m_2)!}. \quad (5)$$

Here l_1 and l_2 are the angular momenta, $\mathbf{j}_1 = \mathbf{l}_1 + \mathbf{s}_1$ and $\mathbf{j}_2 = \mathbf{l}_2 + \mathbf{s}_2$ are the channel spins of the first and the second emitted proton, respectively, and $\mathbf{s}$ and ν denote the proton spin and its projection. The spin-parity of ^{14}O is 0^+ which leads to $j_2 = I_1$. The quantities I and I_1 are spins of resonances in ^{16}Ne and ^{15}F, respectively, $C_{m_1, m_2, m}^{j_1, j_2, j}$ are Clebsch-Gordan coefficients and $P_m^l(\theta)$ the associated Legendre polynomials.

4.2.1 The ^{16}Ne ground state

The experimental correlations for the energy region around the ground state of ^{16}Ne are shown in fig. 7. A simulation based on the calculations within a three-body model [12], where the fractional energy distributions are obtained in both the Y- and T-systems, is compared to fits to the data (dashed line). The shape of the angular distribution in the Y-system is mainly determined by the shape of energy distribution in the T-system, and vice versa. This symmetry is clearly demonstrated in figs. 7, 8 and 9.

Fig. 7. Three-body correlations between the decay products from the ^{16}Ne ground state. Experimental data are shown for fractional energy ((a),(c)) and angular ((b),(d)) correlations in the Y- and T-systems, respectively. The dashed lines are the result of Monte Carlo simulations using the fractional-energy spectra calculated in ref. [12] as input. The solid lines demonstrate the result obtained in the sequential-decay model. In both cases the experimental resolution was taken into account.
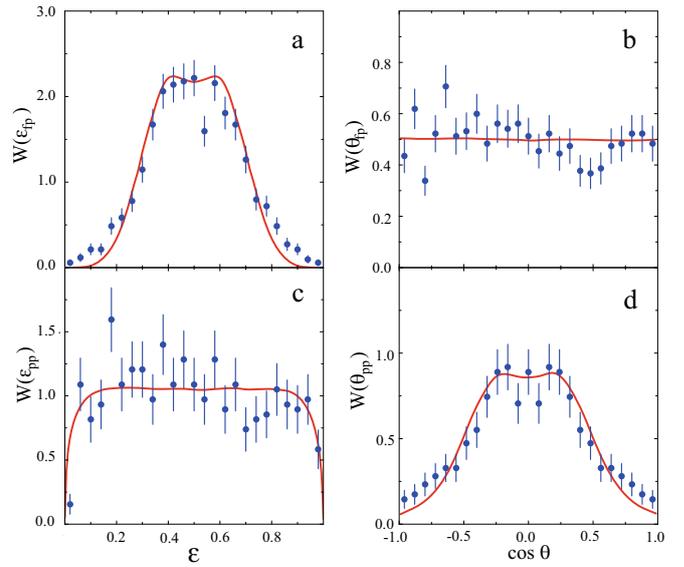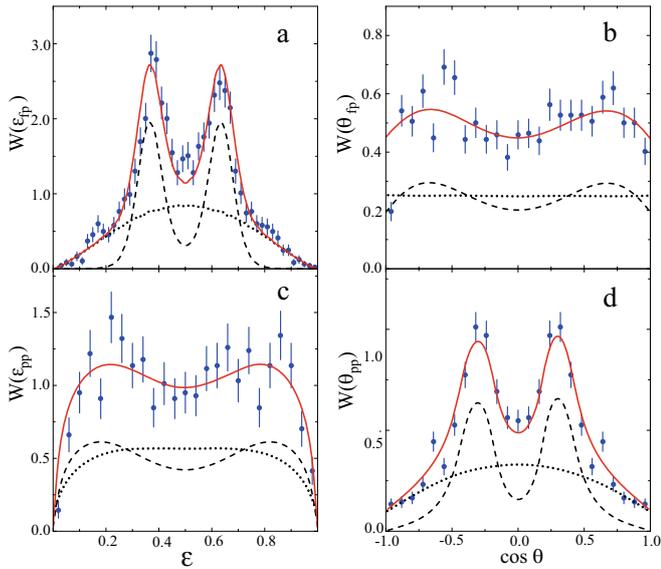

Fig. 8. Three-body correlations between the decay products for the 2^+ state in ^{16}Ne at 3.22 MeV. The notations are the same as in fig. 7. The solid lines display the result of calculations for sequential decay through the ground state of ^{15}F. The experimental resolution was taken into account.

As an example the following relation may be written in the case when $m_f \gg 2m_p$:

$$\cos\theta_{fp} \approx \frac{2\epsilon_{pp}-1}{2\sqrt{\epsilon_{fp}(1-\epsilon_{fp})}}. \qquad (6)$$

The functional dependence is mainly determined by the numerator $2\epsilon_{pp}-1$. The angular distributions in Y-system can thus be reproduced with an acceptable accuracy from the known fractional-energy distributions in the T-system. This is especially true in the case when $W(\epsilon_{fp})$ is a narrow distribution centred at $\epsilon_{fp} = 0.5$.

The dashed lines shown in fig. 7 reproduce qualitatively the four correlation functions. Calculations within a three-body model with a more accurate estimate of the influence from the Coulomb interaction by a classical extrapolation of the momentum distributions, as suggested in ref. [25], would lead to narrower theoretical $W(\epsilon_{fp})$ and $W(\theta_{pp})$ distributions than those presented in ref. [12], and thus to a better description of the experimental data.

The solid lines correspond to calculations for sequential decay through the ^{15}F ground-state resonance by using eqs. (4) and (5). The experimental situation, both concerning the position and width of the ^{15}F(g.s.) resonance, is unclear (see refs. [26–28] and references therein). The experimentally determined position of the resonance varies between 1.23 and 1.60 MeV and its width between 0.7 and 1.2 MeV. For a comparison with the three-body decay model, the calculations for sequential decay were made with the ^{15}F resonance parameters given in ref. [12], $E_r = 1.48$ MeV, $\Gamma = 1$ MeV. Note, that no free parame-

ter was used and also that the sensitivity to the position and width of the ^{15}F(g.s.) is low. It turns out that the experimental correlation functions $W(\epsilon_{fp})$ and $W(\theta_{pp})$ are described perfectly, while $W(\epsilon_{pp})$ and $W(\theta_{fp})$ cannot be reproduced. The reason for this is that the interaction between the two protons in the ^{14}O+p+p system is ignored in the sequential-decay model. The observed effect can, in principle, be explained as a sequential two-proton emission with a pp interaction in the final state. However, as a consequence of the large width of ^{15}F(g.s.), *i.e.* its very short lifetime, and that the internal energy in the three-body system is comparable with this width, the concept of two independent one-proton steps is pointless. Thus, the three-body correlations demonstrate features that point to a democratic decay. In such a decay the interaction between any pair of the decay products is of equal importance [29].

4.2.2 The 3.22 MeV state

Correlations between the decay products from the first excited state are shown in fig. 8. The first excited state in ^{16}Ne decays predominantly to the ^{15}F(g.s.) state, which in turn decays to ^{14}O(0^+) by emission of a proton with angular momentum $l = 0$. The angular distribution $W(\theta_{fp})$ is expected to be isotropic in a sequential decay if the angular momentum of one of the emitted protons is equal to zero. This implies that the initial spin of the decaying state cannot be determined. The results given by the sequential decay model, eqs. (4), are plotted in fig. 8 as solid lines.

Fig. 9. Three-body correlations between the decay products of the $E_r = 7.57(6)$ MeV state in ^{16}Ne. The dashed lines show the result of Monte Carlo simulations using the fractional-energy spectra for sequential decay of a 2^+ state through the $5/2^+$ state in ^{15}F (see text). The physical background (see text) is shown as dotted lines. Their sum is shown as solid lines. The experimental resolution was taken into account.
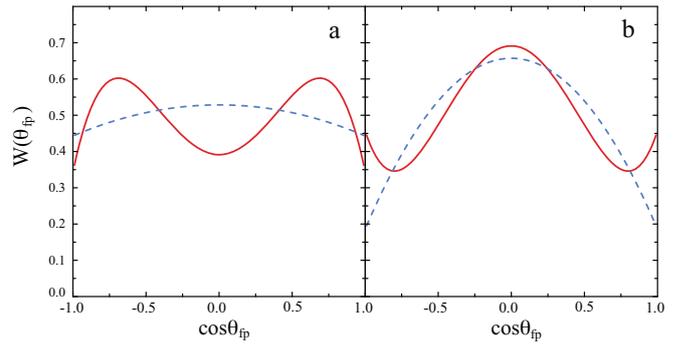
4.2.3 The 7.57 MeV state

Correlations between the decay products from the excited state at the resonance energy 7.57 MeV are shown in fig. 9. The characteristic distributions in $W(\theta_{fp})$ and $W(\epsilon_{pp})$ indicate that the spin and parity of the initial state can be determined.

The two peaks seen in $W(\epsilon_{fp})$ and $W(\theta_{pp})$ can be associated with transitions to either the state at $E_r = 4.8$ MeV or to the one at $E_r = 2.8$ MeV in ^{15}F (the ratios of the ^{15}F resonance energies to the total decay energy is 0.63 and 0.37, respectively. For the decay to the 2.8 MeV state peaks in the ϵ_{fp} spectrum are expected at 0.37 and $1 - 0.37 = 0.63$). Thus there are two alternative choices for the intermediate state. However, the state at 4.8 MeV has spin-parity $I^\pi = 1/2^-$ and it can decay to the ground state of ^{14}O only by emission of a proton with angular momentum $l = 1$. The correlations $W(\theta_{fp})$ and $W(\epsilon_{pp})$ cannot be reproduced in that case.

The sensitivity of the angular distribution with respect to the spin of the ^{16}Ne resonance is demonstrated in fig. 10 where angular correlations (eq. (5)) are shown for two assumed initial spin values $I^\pi = 2^+$ and $I^\pi = 3^+$. A state with spin-parity 3^+ was predicted in ref. [30] to be situated around $E_r = 8$ MeV, close to the energy of the resonance observed here. In both cases, two values for the channel spin are possible $j_1 = 3/2$ and $j_1 = 5/2$ (see footnote[1]). For the second proton, only the channel spin $j_2 = 5/2$ is possible. The $j_1 = 3/2$ and $j_1 = 5/2$ decays differ, how-

---

[1] $j_1 = 1/2$ is also possible but this would result in an isotropic distribution.

Fig. 10. Angular correlations between the decay products of the ^{16}Ne $E_r = 7.57(6)$ MeV state decaying by sequential emission of protons through the intermediate $5/2^+$ state in ^{15}F. Panel (a) shows the case for an assumed ^{16}Ne(2^+) state and panel (b) for a ^{16}Ne(3^+) state. The solid lines correspond to the channel spin $5/2^+$, and the dashed lines to spin $3/2^+$.

ever, drastically and only the choice of $I^\pi = 2^+$, $j_1 = 5/2$ can explain the observed distribution. The final result of the calculations using eqs. (4) and (5) and initial spin 2^+ is shown in fig. 9 as dashed lines.

The physical background arising from the assumed unresolved resonances was determined by analysing the shapes of the correlations in the neighbouring energy regions to the left and right sides of the resonance. These background contributions are shown in fig. 9 as dotted lines. The result of the calculations described above is shown as dashed lines and the sum of these two contributions (solid lines) agrees well with the experimental data. No sign of a transition to the ground state of ^{15}F can be observed in the correlation functions.

Thus, we are faced with a case where the initial 2^+ state emits a proton from the $d_{5/2}$ shell feeding the ^{14}O plus proton in a $d_{5/2}$ shell configuration in ^{15}F. This parent 2^+ state is unstable towards emission of two protons by 7.57(6) MeV and its width is surprisingly narrow. Thus, its structure cannot be as simple as a ^{14}O+p+p state. It is also situated above the threshold for emission of four protons by 1 MeV (see fig. 6). This indicates a possible many-body structure and the narrow width may be connected to ^{12}C+4p configuration with four protons in the (sd) shell (*e.g.*, see ref. [31]). A special case of such a structure could consist of an excited core together with two protons, ^{14}O(2^+)+2p, proposed in refs. [7,8]. The 2^+ state in ^{14}O at $E^* = 6.609(10)$ MeV is unstable towards proton emission by 2 MeV and its width is ≤ 5 keV [32]. Note also that the theoretical predictions for the position of the second 2^+ state in ^{16}Ne resulted in $E^* = 4.2$ MeV [30] or $E^* = 3.67$ MeV [33], both close to the known position of the second 2^+ in the mirror nucleus ^{16}C, $E^* = 3.99$ MeV (see fig. 6). Comparison with the mirror nucleus ^{16}C (see fig. 6) suggests it to be the third 2^+ state in ^{16}Ne.

Finally, we note that none of the three-body correlations obtained in the present experiment reveal any features of strong angular and energy correlations between the two protons, which could be attributed to a decay proceeding as di-proton emission.

Table 2. Coefficients in the isobaric multiplet mass equation obtained from a fit to experimental data.

State	a (keV)	b (keV)	c (keV)	$\chi^2_{\min}/1$	Prob.
0^+	17982(3)	−2572(4)	213(2)	3.29	7%
2^+	19771(8)	−2598(10)	220(4)	3.68	6%

5 Thomas-Ehrman shifts in the T = 2, A = 16 multiplet

The progress in the spectroscopy of exotic nuclei has given access to several isospin multiplets. Investigation of isospin symmetry in the isobaric analog states and the properties of the Isobaric Multiplet Mass Equation (IMME) was recently made in refs. [34,35]. Isospin symmetry means that the strength of the strong interaction between any pair of nucleons is the same, independent of whether they are protons or neutrons. The violation of isospin invariance resides in the electromagnetic interaction, which removes the state degeneracy by splitting the distances between states with identical quantum numbers with the exception of their isospin projection. Assuming a two-body Coulomb force for the perturbation, the masses of isospin multiplet members should follow a quadratic form:

$$M(\alpha, T, T_z) = a(\alpha, T) + b(\alpha, T)T_z + c(\alpha, T)T_z^2. \quad (7)$$

Here, the isobaric states are denoted (α, T, T_z) where α stands for the relevant quantum numbers (I^π, A). The coefficients, a, b, and c can be determined from experiments.
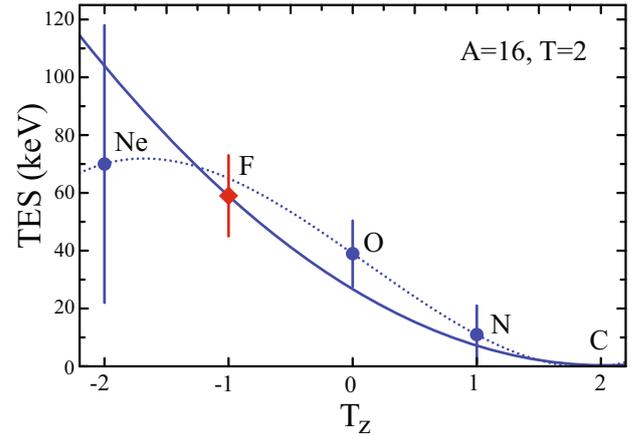
Isospin invariance broken by a non-electromagnetic interaction would result in higher order terms in eq. (7). Such higher-order effects arise in particular from the interaction between neighbouring states of different isospins. Such terms reflect the amount of isospin mixing.

We now turn to an IMME analysis using the known masses of the $A = 16$ quintet. The ground-state masses were taken from AME2012 [36], while the mass excesses of the excited states were taken from the TUNL evaluation [37]. The fit was made by using the experimental data for ^{16}Ne, ^{16}O, ^{16}N, and ^{16}C only, since there is no experimental information about ^{16}F. Table 2 gives the result of a least square fit to the masses of the 0^+ and 2^+ states. The $\chi^2_{\min}$ is given together with the estimated probability to have χ^2 larger than $\chi^2_{\min}$ when the hypothesis of a quadratic form of IMME is true. The obtained probabilities in the last column in table 2 are, however, not small enough to completely rule out the necessity to include higher-order terms.

With these coefficients we may predict the energies of the unknown excited $T = 2$ states in ^{16}F:

− a 0^+ state at $E^* = 10.087(10)$ MeV and
− a 2^+ state at $E^* = 11.908(14)$ MeV.

The prediction for the ^{16}F(0^+) state is in good agreement with the estimate made by Fortune [38]. An inclusion of a cubic T_z term in IMME results in the same values within

Fig. 11. Thomas-Ehrman shift between 2^+ and 0^+ states for members of the isobaric quintet ($A = 16$, $T = 2$) as a function of the the isospin projection. The energy shift was calculated relative to ^{16}C, with the 2^+ to 0^+ energy difference of 1762 keV. The experimental data are shown as filled circles. The solid line is obtained from the fits to the quadratic IMME (eq. (7)) of the 0^+ to 2^+ states given in table 2. The dotted line shows the result when a T_z^3 term is included in eq. (7). The predicted value for ^{16}F is shown as a rhombus, and amounts to 59 keV.

the statistical uncertainty. The fit made with eq. (7) allows to see how the TES varies as a function of the isospin projection. The experimental data are in fig. 11 shown as filled circles.

The TES was determined as changes in distances between 2^+ and 0^+ states in ^{16}Ne relative to those in ^{16}C. The rhombus displays the predicted value for ^{16}F. The full drawn curve in fig. 11 shows the TES using the coefficients in table 2, while the dashed line shows the result after adding a cubic term to eq. (7). A systematic increase of the TES with decreasing T_z is observed.

6 Summary

The mechanism of two-proton emission from the ground state and two excited states in ^{16}Ne have been studied by analysing correlations between the ^{14}O+p+p decay products. This paper is the first to report the decay details of all of the three observed states in ^{16}Ne and represents the most complete study of unbound nucleus so far.

The energy and the width ^{16}Ne(g.s.) were obtained with significantly improved precision, and it was found that its decay can be considered as democratic.

The first excited state decays by sequential emission of protons through the broad ^{15}F(g.s.) resonance ($\Gamma \approx 1$ MeV).

The narrow state previously observed at 7.6 MeV above threshold is confirmed and the present data are able reduce the upper limit of its width by an order of magnitude. The fractional energy and angular correlations are well described assuming emission of a proton from the $d_{5/2}$ shell to the ^{15}F($5/2^+$) state ($E_r = 2.76$ MeV), which in turn decays by proton emission from the $d_{5/2}$ shell to ^{14}O.

The spin-parity of the $E_r = 7.57\,\mathrm{MeV}$ state was in this way unambiguously identified as $I^\pi = 2^+$ and from mirror symmetry assigned as the third 2^+ state in $^{16}\mathrm{Ne}$. The implied $(d_{5/2})^2$ proton nature for this state is not able to explain its surprisingly small width, suggesting a more complicated aspect to its structure.

The error-weighted mean energies of the ground state and the first excited state in $^{16}\mathrm{Ne}$ were obtained by using all available experimental data. This gave the Thomas-Ehrman shift between the 2^+ and 0^+ states in the mirror nuclei $^{16}\mathrm{Ne}$ and $^{16}\mathrm{C}$, to be $\Delta(2^+, 0^+) = +70(46)\,\mathrm{keV}$.

References

1. F. Wamers *et al.*, Phys. Rev. Lett. **112**, 132502 (2014).
2. R.J. Holt *et al.*, Phys. Lett. B **68**, 55 (1977).
3. G.R. Burleson *et al.*, Phys. Rev. C **22**, 1180 (1980).
4. K. Föhl *et al.*, Phys. Rev. Lett. **79**, 3849 (1997).
5. G.J. KeKelis *et al.*, Phys. Rev. C **17**, 1929 (1978).
6. C.J. Woodward, R.E. Tribble, D.M. Tanner, Phys. Rev. C **27**, 27 (1983).
7. I. Mukha *et al.*, Phys. Rev. C **79**, 061301 (2009).
8. I. Mukha *et al.*, Phys. Rev. C **82**, 054315 (2010).
9. K.W. Brown *et al.*, arXiv:1406.3285v2 [nucl-ex] (2014).
10. V. Guimarães *et al.*, Phys. Rev. **58**, 117 (1998).
11. F. James, M. Roos, Comput. Phys. Commun. **10**, 343 (1975).
12. L.V Grigorenko *et al.*, Phys. Rev. Lett. **88**, 042502 (2002).
13. M. Petri *et al.*, Phys. Rev. C **86**, 044329 (2012).
14. A.H. Wuosmaa *et al.*, Phys. Rev. Lett. **105**, 132501 (2010).
15. Y. Satou *et al.*, Phys. Lett. B **728**, 462 (2014).
16. K. Ogawa *et al.*, Phys. Lett. B **464**, 157 (1999).
17. R.G. Thomas, Phys. Rev. **88**, 1109 (1952).
18. J.B. Ehrman, Phys. Rev. **81**, 412 (1951).
19. H.T. Fortune, Phys. Lett. B **718**, 1342 (2013).
20. E. Comay, I. Kelson, A. Zidon, Phys. Lett. B **210**, 31 (1988).
21. S. Aoyama, Phys. Rev. C **62**, 034305 (2000).
22. E. Garrido, D.V. Fedorov, A.S. Jensen, Phys. Rev. C **69**, 024002 (2004).
23. F.C. Barker, Phys. Rev. C **59**, 535 (1999).
24. D.F. Geesaman *et al.*, Phys. Rev. C **15**, 1835 (1977).
25. L.V. Grigorenko, M.V. Zhukov, Phys. Rev. C **68**, 054005 (2003).
26. V.Z. Goldberg *et al.*, Phys. Rev. C **69**, 031302 (2004).
27. A. Lepine-Szily *et al.*, Nucl. Phys. A **734**, 331 (2004).
28. F.Q. Guo *et al.*, Phys. Rev. C **72**, 034312 (2005).
29. R.I. Jibuti, N.B. Krupennikova, V.Yu. Tomchinsky, Nucl. Phys. A **276**, 421 (1977).
30. N.K. Timofeyuk, P. Descouvemont, Phys. Rev. C **81**, 051301 (2010).
31. H.T. Fortune, R. Sherr, Phys. Rev. C **87**, 057308 (2013).
32. A. Negret *et al.*, Phys. Rev. C **71**, 047303 (2005).
33. H.T. Fortune, R. Sherr, Phys. Rev. C **82**, 027310 (2010).
34. M. MacCormik, G. Audi, Nucl. Phys. A **925**, 61 (2014) **925**, 296(E) (2014).
35. Y.H. Lam *et al.*, At. Nucl. Data Tables **99**, 680 (2013).
36. M. Wang *et al.*, Chin. Phys. C **36**, 1603 (2012).
37. D.R. Tilley, H.R. Weller, C.M. Cheves, Nucl. Phys. A **564**, 1 (1993).
38. H.T. Fortune, Phys. Rev. C **74**, 054310 (2006).